Application of a Switching Control Strategy to Extract Energy from Turbulence by a Fixed-wing UAV

F. Pasquali, Y. Brière *, and N. Gavrilovic
Université Federale de Toulouse - ISAE Supaero, 10 av. Edouard Belin, 31400 Toulouse, France

http://www.imavs.org/

ABSTRACT

The objective of this paper is to design a control law to allow a small fixed-wing Unmanned Aerial Vehicle to extract energy from atmospheric turbulence. From literature data the properties of atmospheric gusts at low altitude are discussed and a single point measurement is proved to be representative of the wind field. The longitudinal flight dynamics of the aircraft is analyzed and the phugoid mode is found to be the main driver of the energy extraction process. A switching controller that places the poles of the phugoid mode depending on the instantaneous variation of energy of the aircraft is designed. Statistical simulations show an increase of energy of the aircraft when this strategy is applied.

1 INTRODUCTION

A major problem of Unmanned Aerial Vehicles consists in the duration of the battery, which nowadays strongly reduces the endurance of a mission; anyway, the atmosphere containts energy in the form of wind. While the energy in everyday gusts is negligible compared to the one of a civil airplane [1], it represents a large quantity of the energy of small UAVs, whose flight domain is close to the one of a bird, thus making energy extraction worth to be investigated.
Energy harvesting from turbulence is not a topic with well-defined boundaries and results, thus several research domains have to be taken into account. First, the experience of glider pilots [2, 3] and the flight of birds are a source of data. Second, in the '90s, several authors [4, 5, 6] addressed the response of civil planes to gusts (for strong winds due to extraordinary meteorological conditions) in particular in the phases of take-off and landing, leading to the Total Energy Control System (TECS), common on civil aircrafts nowadays. Specifically about energy harvesting from the atmosphere, the literature have dealt with three phenomena: thermals [7] that are widely known by glider pilots, wind shear which is exploited by marine birds via a technique called 'dynamic soaring' [8] and eventually gusts. For the first two cases, an apriori knowledge of the wind field is used, contrary to the stochastic nature of turbulence.
Two approaches are common to deal with atmospheric gusts. One is to investigate the natural capability of the wing to extract energy, in terms of "microlift" force [9], aeroelastic response [10] and overall design [11]. The other is to implement a suitable control law; the most used technique [12, 13, 14, 15] computes a set of feedback gains via optimization of the energy of the aircraft on a set of gusts.

The main contributions of this paper are:

1. The evidence that a single point measurement of the wind field is representative of the energetic turbulent wind, thus just one probe is needed.
2. The computation of the transfer functions from the turbulent wind velocity to the energy of the aircraft and the identification of the phugoid as the main dynamics affecting this process in the case of horizontal gusts.
3. The design of an energy extraction control law that does not rely on numerical optimization but on the switching between two controllers to tune the pulsation of the phugoid dynamics depending on the instantaneous loss or gain of energy by the aircraft (and the proof of its stability).
4. The simulations on Von Karman horizontal gusts to show that the controller is able to extract energy from gusts without a consistent increase of the elevator activity with respect to a just stabilizing controller

The paper is structured as follow. In 'Section 2' the main results and problems of an optimal control technique are presented. 'Section 3' is dedicated to the analysis of low altitude atmospheric turbulence. 'Section 4' deals with flight mechanics in presence of wind gusts. In 'Section 5' we design the control law and eventually, in 'Section 6' we perform simulations on gusts.

2 LITERATURE REVIEW

The main references dealing with energy extraction from wind gusts using an appropriate control law are the works by Langelaan [12] and Patel et al [15]. They use similar methods to optimize the gains of a proportional feedback law on a set of gusts so to obtain the smallest decrease of energy while gliding. Patel [15] focuses on vertical gusts using a point-mass glider model and proves his results by flight tests. He introduces the idea to use a feedback law depending on the energy and obtains a reduction of energy losses of 36% with respect to a stabilizing controller. Langelaan [12] uses the complete longitudinal rigid dynamics, takes into account vertical and horizontal gusts acting at the same time on the aircraft and proves a reduction of energy losses of around 40%.

*Email address(es): contact yves.briere@isae.fr

http://www.imavs.org/

Even if their results are promising, the usage of an optimal control strategy leads to some unclear points.

1. Langelaan [12] obtains a set of optimal gains that show a large scatter and sometimes changes in sign when the optimization is performed on different sets of gusts.
2. The relations among the characteristics of the aircraft, the properties of turbulence and the control strategy are difficult to be analyzed using numerical methods, so the quantities that have primary importance in the energy extraction process are not identified.
3. When applying the energy extraction control law, a large increase in the control action is required, thus a high amount of power from the batteries is necessary.

3 ATMOSPHERIC TURBULENCE AT LOW ALTITUDE

3.1 What do we mean by turbulence?

The aim of this section is to describe turbulence so to represent an input for our airplane model. Turbulence, due to its "randomness", can be addressed only in a statistical way: several works in the literature, nicely reviewed in [16], measure the Power Spectral Density (PSD) of the wind. We deal only with the turbulent range (at higher frequencies than the spectral gap identified in [17]), while the low frequency phenomena are considered to create a constant wind; when referring to turbulent wind speed, we consider the oscillations of velocity (having zero mean value) with respect to the constant wind. Only the turbulence in the vertical plane is considered, since we investigate only the longitudinal dynamics of the plane.
Common turbulent spectra such as Von Karman [18] or Dryden depend on four parameters:

1. Variance of the turbulent velocity σ^2: corresponding to the total power of turbulence.
2. Injection length L: a measure of the scale of the energetic turbulent eddies (it represents the autocorrelation length of turbulent velocity in a certain direction).
3. Direction with respect to the constant wind: the mathematical representation of the spectrum and the values of variance and injection length in the longitudinal (parallel to the constant wind) and lateral (perpendicular to the constant wind) directions are different.
4. Magnitude of the nominal airspeed ${v_a}^{nom}$ of the aircraft: necessary to translate the turbulent spectra given in terms of wavenumber κ [rad/m] (in the space domain) into pulsation $\Omega = \kappa {v_a}^{nom}$ [rad/s] (time domain), so to represent the evolution in time of the gust felt by the aircraft.

In the case of one dimensional Von Karman gust field in the vertical plane, flying parallel to the constant wind direction, the spectra of the turbulent velocity are $S_x(\Omega)$ 1 (horizontal) and $S_z(\Omega)$ 2 (vertical).

$$S_x(\Omega) = \frac{{\sigma_x}^2 L_x}{\pi {v_a}^{nom}} \frac{1}{(1 + (1.339 L_x \Omega / {v_a}^{nom})^2)^{5/6}} \qquad (1)$$

$$S_z(\Omega) = \frac{{\sigma_z}^2 L_z}{\pi {v_a}^{nom}} \frac{3 + 8(1.339 L_z \Omega / {v_a}^{nom})^2}{(1 + (1.339 L_z \Omega / {v_a}^{nom})^2)^{11/6}} \qquad (2)$$

The difference between Von Karman and Dryden spectra is in the capability to approximate small scales of turbulence, in favor to the Von Karman one. Since we are interested in energetic scales (the largest of turbulence) this distinction is negligible for the design of the control strategy.

3.2 Flight environment

We are interested in flying at altitudes around 100 meters from the ground, in "countryside" and "small city" environments, where there are not major obstacles such as hills or large buildings. Even in absence of local obstacles, there are many large scale meteorological phenomena, such as air stability [19], that have strong influence and could lead to actual turbulence very different from the modelled one: the control strategy has to be very robust to unexpected gusts. Exaustive tables containing measured values of turbulent variance and injection length are reported in [20]. Notice that they declare an uncertainty of about 30% on the spectrum shape, in particular at low frequencies. Named w_x the turbulent wind component in the direction parallel to the constant wind field (horizontal) and w_z the vertical one, in 'Table 1' the typical parameters for the aforementioned terrain conditions are reported and in 'Figure 1' an example of horizontal spectrum and corresponding gust is shown.

	Standard deviation [m/s]	Injection length [m]
w_x	1.5/2.2	320/425
w_z	0.8/1.2	30/40

Table 1: Standard deviation and injection length in countryside and small city environments, from [20]

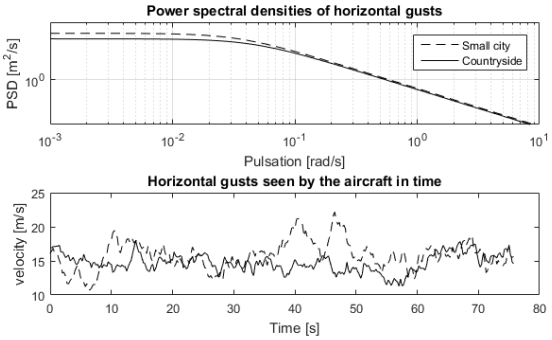

Figure 1: Horizontal wind w_x in frequency and time for 'small city and 'countryside environments

3.3 Scale comparison of turbulence and aircraft

The wingspan of a typical small fixed-wing drone is in the order of 1 meter (for instance in the model used in [12] it is around 4 meters) which is significantly smaller than the injection length scale, thus it is meaningful to model the effect

http://www.imavs.org/

of energetic turbulence on the plane by its value in a single point [16] (even though smaller turbulent wavelength whose impact changes along the wingspan have to be considered for the stabilization of the aircraft [21]). Moreover we compare the time that is needed by the plane to go through an energetic turbulent structure with the time constant of the slowest longitudinal mode of the aircraft (the phugoid) so to assess if the plane is able to respond to the turbulent input. The energetic turbulence time is obtained by dividing the injection length by the airspeed of the plane (a reasonable value for small UAVs is 20 m/s) thus obtaining 16 s / 21 s for the horizontal turbulent component and 1.5 s / 2 s for the vertical one. The time constant of the plane is calculated as the inverse of the phugoid pulsation for the Langelaan [12] model and it results to be 1.8 s. We conclude that the plane is capable to follow easily horizontal gusts, but it could require a strong control action in order to change its attitude to respond to a vertical gust.

4 AIRCRAFT MODEL

4.1 Longitudinal dynamics

The longitudinal dynamics equations 13-15 in [12] are used, where the airspeed is separated from the velocity of the wind with respect to the ground. The coefficients are adapted from [12]: for the sake of simplification, we consider a parabolic polar, the thrust aligned with the airspeed and the lift coefficient independent from the derivative of angle of attack. From the longitudinal dynamics in presence of wind, the expression of the total energy 3 (of the longitudinal dynamic) of the aircraft can be obtained, where v_g and h stand for the velocity and the altitude in the ground frame. The energy stored in the rotations is not considered because these should be limited.

$$\begin{aligned} E &= -gh + 1/2m{v_g}^2 \\ &= -gh + 1/2[(v_a\cos(\gamma) + w_x)^2 + (v_a\sin(\gamma) - w_z)^2] \end{aligned} \tag{3}$$

4.2 Linerarization of the dynamics

The equations are linearized around the stability point given by a nominal airspeed of ${v_a}^{nom} = 20$ m/s, null flight path angle and pitch rate. We use the state vector 4 that is composed (in this order) by the variations from their nominal value of airspeed, flight path angle, angle of attack and pitch rate (four variables that are a common choice to represent the longitudinal dynamics), altitude (which is necessary to compute the potential energy) and integration of the wind gradient in horizontal and vertical directions (because the total energy variation of the aircraft depends on them). Notice that w_x and w_z do not take into account the constant wind field. The input vector 5 is composed by four variables: thrust and elevator commands and the wind gradients in horizontal and vertical directions. While we are able to control the first two, the latter have to be considered as disturbances (with known spectrum). The output vector 6 is the energy, linearized from 3.

$$x = \begin{bmatrix} \delta v_a & \delta\gamma & \delta\alpha & \delta q & \delta h & \delta w_x & \delta w_z \end{bmatrix}^T \tag{4}$$

$$u = \begin{bmatrix} \delta T & \delta e & \dot{w_x} & \dot{w_z} \end{bmatrix}^T \tag{5}$$

$$E_{linear} = -g\delta h + {v_a}^{nom}\delta v_a + {v_a}^{nom}\delta w_x \tag{6}$$

The numerical value of the coefficients is computed from [12] (the full state space matrices are in 'appendix A') and it leads to a poorly damped phugoid, thus, before considering the energy extraction process, a stabilizing controller is needed. This is designed via pole placement technique, the airspeed and the flight path angle (the phugoid mode is a combination of these two variables) are feedbacked through two gains to the elevator in order to obtain a damping of 0.7 (the frequency is kept to its natural value). Via simulations we assess that this stabilizing controller does not interfere with the energy extraction process (the energy of the aircraft oscillates around its nominal value in presence of gust disturbance).

4.3 Phugoid approximation

We investigate if the phugoid approximation of the longitudinal dynamics is valid to represent the effect of the wind on the aircraft. The Bode plots of the transfer functions from the wind gradients to the energy (and to the other state variables) are coincident for all frequencies a part of a small range close to the short period mode pulsation. It is thus reasonable to use the phugoid approximation for the design of the control law and to reduce the order of the system; this result is in accordance with the observations made in [22] . The new state 7 is composed by the airspeed, flight path angle, altitude and the integration of the horizontal and vertical turbulent wind (the state matrices are in 'appendix B').

$$x^{phugoid} = \begin{bmatrix} \delta v_a & \delta\gamma & \delta h & \delta w_x & \delta w_z \end{bmatrix}^T \tag{7}$$

4.4 Energy analysis

From the linear model we obtain the transfer functions from the horizontal and vertical wind to the energy, in 'Figure 2'. The vertical wind to energy transfer functions has the shape of an integrator, where the main contribution to the energy is due to the vertical displacement, while the characteristics of the plane have a small influence on this process. The horizontal wind to energy transfer functions has a low pass behavior whose cut off frequency is close to the phugoid one: we deduce that by tuning the phugoid mode characteristics, the energy extraction process can be modified. In the following, we focus only on the energy extraction process from horizontal gusts and we aim at designing a controller acting on the phugoid mode.

It is possible to compare the effect of the thrust and the horizontal wind gradient. The columns in the input matrix $B^{phugoid}$ (in 'appendix B') corresponding to the thrust (first) and the horizontal wind gradient (third) have the same effect (a part of a minus sign) on the dynamics of the airspeed and

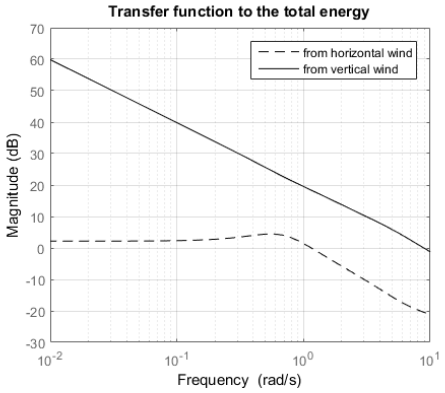

Figure 2: Bode magnitude plots of the transfer functions from the horizontal and vertical wind to the energy

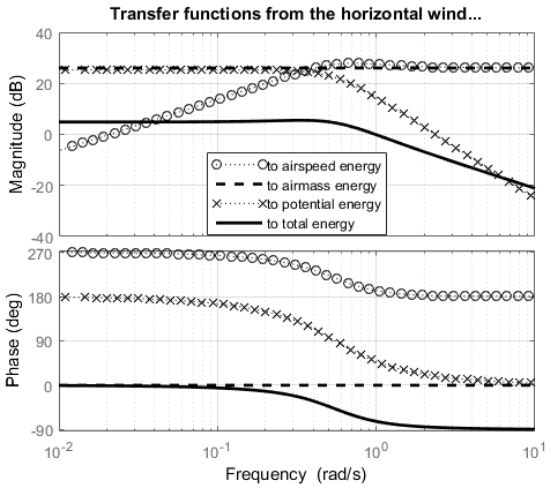

Figure 3: Bode plot of the transfer functions from the horizontal wind gradient to the components of the total energy

the flight path angle, thus allowing us to treat wind gradients as a source of additional propulsion. Their effect on the overall energy of the plane is neverthless different, since the integration of wind, but not the one of the thrust appears in 3. The same conclusion is obtained experimentally in [23].
The linear expression of the energy 6 is composed by three terms that we name, slightly modifying the convention in [4]:

1. Airspeed energy: $E_{airspeed} = {v_a}^{nom}\delta v_a$
2. Potential energy: $E_{potential} = -g\delta h$
3. Airmass energy: $E_{airmass} = {v_a}^{nom}\delta w_x$

When a stabilizing controller is used to keep a constant airspeed, all the energy coming from the wind will be converted into altitude gain. From 'Figure 3', we assess which is the dominant contribution at a certain pulsation of the gust and how energy passes from one component to the other.

1. Airmass energy is a constant gain so its contribution is constant over all the frequencies.
2. Airspeed energy shows a high pass behavior (whose cut-off frequency is the phugoid one) so to counterbalance the airmass energy at high frequencies (the wind variation is seen only as a variation of airspeed, since the inertial velocity of the plane does not have time to change).
3. Potential energy has a low pass behavior and it counterbalances the airmass energy at low frequencies (the controller is able to stabilize the airspeed around its nominal value).

4.5 Static gain of the wind-to-energy transfer function

The pole placement controller (used before for stabilization) allows us to change the phugoid pulsation, while keeping its damping at 0.7. Numerically we find a relation between the static gain of the horizontal wind-to-energy transfer function and the phugoid frequency, as in 'Figure 4', and its effect in the time domain is shown in 'Figure 5'. This property allows us to act on the shape of the horizontal wind-to-energy transfer function by tuning a feedback controller from airspeed and flight path angle to the elevator ('Figure 6'), with an approach similar to the one used in H-infinity technique.

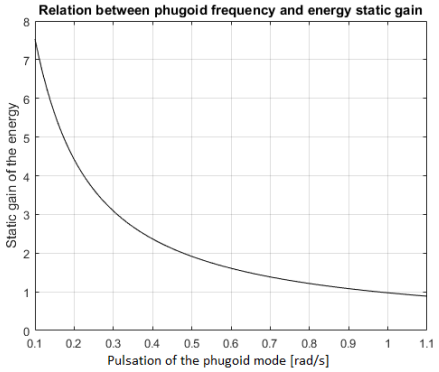

Figure 4: Relation between the static gain of the wind-energy transfer and the phugoid frequency (given a damping of 0.7).

5 CONTROL STRATEGY

5.1 Overview on the control architecture

The objective of the control law is extracting energy from gusts. The innovation present in this work consists in using a feedback law that switches between two sets of gains depending on the energy derivative of the aircraft to control the elevator action, as in 'Figure 7'.
When the aircraft is gaining energy, we exploit it as much as possible, while, when it loses it, we aim at losing the smallest quantity. This translates into having large oscillations of energy (high gain of the wind-energy transfer function) when it

http://www.imavs.org/

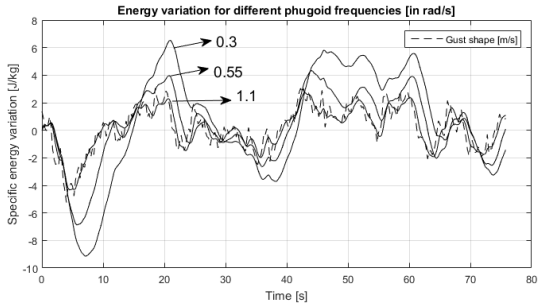

Figure 5: Effect of tuning the phugoid frequency in the time domain.

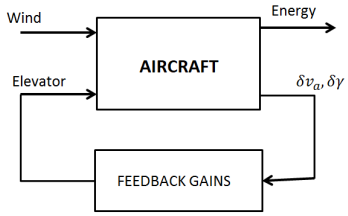

Figure 6: Representation of the system and the pole placement controller.

is entering the plane and very small ones when it is exiting the system (small gain of the wind-energy transfer function). Notice that we do not try to invert the natural energy exchange process (from losing to gaining energy) but we act only on the amplitude of it.

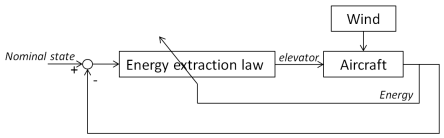

Figure 7: Overview of the architecture.

5.2 *Phugoid pole placement technique*

We exploit the relation found between the phugoid frequency and the static gain of the system in 'Figure 4' to achieve the aforementioned objective. Since the turbulent injection frequency is sensibly lower than the frequency range where we move the phugoid poles, the static gain corresponds to the gain at the injection frequency. To place the phugoid frequency the pole placement method of a second order system is used, and the gains become dependent on the energy derivative 8, where ${k_1}^{in/out}$ represents the gain computed respectively for the "entering" (in) and "exiting" (out) energy law and E is 3. The same rule is valid for the gain k_2. The magnitude Bode plots of the two switched subsystems are in 'Figure 8' and the schematic representation of this law is in 'Figure 9'.

$$\delta e = k_1(dE/dt)\ \delta v_a + k_2(dE/dt)\ \delta\gamma$$
$$k_1(dE/dt) = \begin{cases} {k_1}^{in} & \text{if } dE/dt \geq 0 \\ {k_1}^{out} & \text{if } dE/dt < 0 \end{cases} \quad (8)$$

The set of phugoid frequency pairs $(\omega_{in}, \omega_{out})$ among whom we can choose for our control strategy is limited by the validity of the phugoid approximation (in the direction of higher frequencies), by the non-linear effects present in the realistic model (for lower frequencies) and by the stability of the switched system (when the difference between the two frequencies becomes too large, as it will be discussed in 'subsection 5.4').

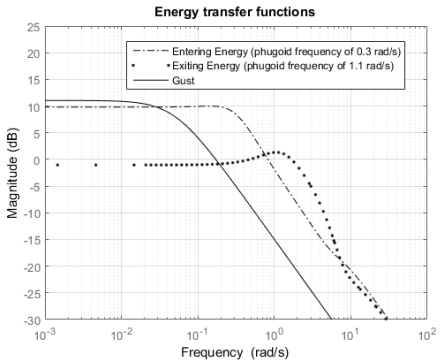

Figure 8: Magnitude of the closed loop transfer functions between the horizontal turbulent wind and the energy (dotted lines) when we place the phugoid poles, for instance, at 0.3 rad/s ("entering" energy mode) and 1.1 rad/s ("exiting" energy mode). The solid line is the transfer function representing the Dryden turbulent spectrum.

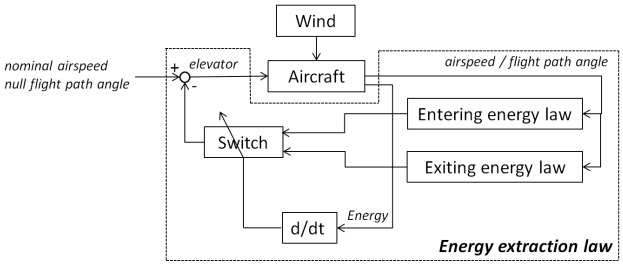

Figure 9: Energy extraction control strategy.

5.3 *Switched system formalism*

We can classify the controlled system that is obtained as belonging to the class of autonomous switched system with externally forced switching [24]. Turbulence is an external disturbance, the elevator action is hidden in the modification of the phugoid dynamics and the thrust input is not used, thus the only way to control this system is to act on the switching signal. Moreover, the mode sequence is fixed, since we are switching between only two systems (even though it would

http://www.imavs.org/

http://www.imavs.org/

have been possible to design more than two modes, we chose two to stick with physical reasoning). The switched system can be represented by 9, where the states are continuous across switching instants and $\sigma(t)$ is the switching signal. In our case $\sigma(t)$ is not an explicit function of time but of the states and it can only assume binary values (in or out), meaning the system is in the "entering" or "exiting" energy mode. We introduce the notation ${A_{\sigma(t)}}^{phugoid}$ 10 to represent a matrix that assumes the values of the phugoid state matrix with pulsation ω_{in} or ω_{out} depending on $\sigma(t)$.

$$\dot{x} = \begin{bmatrix} {A_{\sigma(t)}}^{phugoid} & \begin{matrix} 0 & 0 \\ 0 & 0 \end{matrix} \\ \begin{matrix} 0 & -20 \\ 0 & 0 \end{matrix} & \begin{matrix} 0 & 0 \\ 0 & 0 \end{matrix} \end{bmatrix} x + \begin{bmatrix} -1 \\ 0 \\ 0 \\ 1 \end{bmatrix} \dot{w}_x \tag{9}$$

$$A^{phugoid}_{\sigma(t)} = \begin{cases} A^{phugoid}_{in} & \text{if } dE/dt \geq 0 \\ A^{phugoid}_{out} & \text{if } dE/dt < 0 \end{cases} \tag{10}$$

5.4 *Switched system stability*

We are interested in guaranteeing the stability of the airspeed and the flight path angle dynamics (since our objective is to have an "unstable" altitude) in the case of arbitrary switching, in fact, even if the two subsystems between whom we switch are stable, this is not sufficient to prove the stability of the overall switched system. We apply theorem 3.1 in [25], which gives a necessary and sufficient condition to have a Common Lyapunov Quadratic Function for a pair of switched second order stable linear time invariant systems (such as the phugoid representation). In 'Figure 10' the stability domain is shown, depending on the phugoid pulsations for the entering and exiting energy case. We choose the stable couple $(\omega_{in}, \omega_{out}) = (0.3, 1.1)$ rad/s in order to perform simulations, but we cannot assess apriori its performances in terms of energy extraction (there could be stable couples giving better performances).

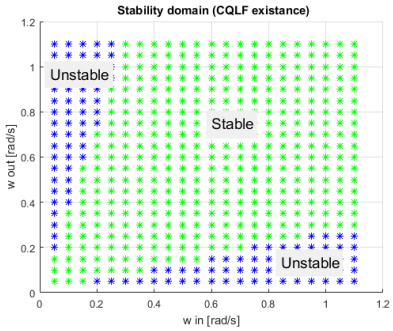

Figure 10: Stability domain of the switching system, expressed in function of the entering (in) and exiting (out) phugoid pulsations.

6 SIMULATIONS

6.1 *Energy evolution in time*

The capability of our strategy to extract energy from gusts is assessed by simulations on a non-realistic sinusoidal gust of low frequency (0.05 rad/s, in 'Figure 11') and on realistic Von Karman gusts. In both cases we are able to obtain an increase in energy with respect to the stabilizing controller. A great advantage of our technique is that the control action is not significantly increased (and so the energy of the battery cunsumed by the actuators) with respect to the one needed for stabilisation purposes only ('Figure 12'), contrary to the results in [12].
We can simulate on the same gust different pairs of phugoid frequencies ('Figure 13'); as expected from 'Figure 4', when the difference between the entering and exiting phugoid frequencies is increased, the extracted energy increases as well. Further insights are necessary to understand the relation between the chosen frequencies and the achievable energy increase.

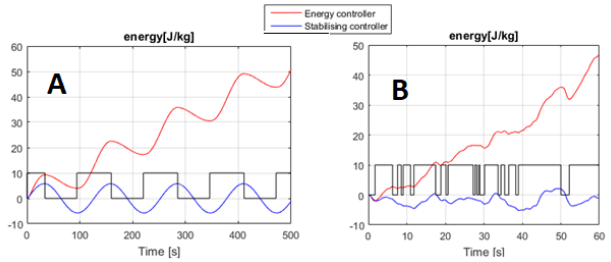

Figure 11: Energy evolution and switching signal in the case of sinusoidal (A) and Von Karman (B) gust. The "energy extraction" controller is compared to a simple stabilizing controller. The black line is the switching signal (a relay could be needed to avoid fast switching).

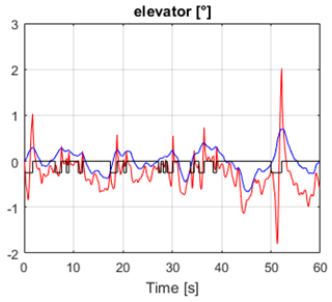

Figure 12: Elevator deflection for the energy extraction controller (red) compared to its usage by the stabilizing controller (blue).

6.2 *Statistical simulations*

We simulate our control strategy applied to the non-linear longitudinal rigid aircraft model on a set of Von Karman horizontal gusts, for the phugoid frequencies chosen in 'subsection 5.4'. A set of 200 gusts (100 representative of "countryside" environment and 100 of the "small city" one) of 60 seconds each are used ('Table 2'). We can estimate the achievable reduction of thrust ΔT from the amount necessary to fly in still air (where the airspeed is the ground speed too) corre-

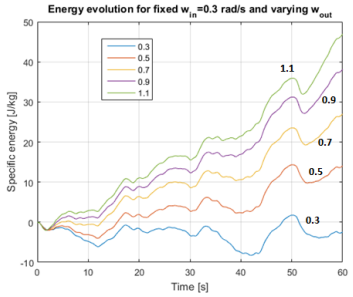

Figure 13: Effect of the variation of ω_{out} for the same gust.

sponding to the extracted power $P_{extracted}$ in 11.

$$P_{extracted} = \Delta T {v_a}^{nom} \tag{11}$$

	Countryside	Small city
Extracted energy [J/Kg]	40.25 ± 7.98	51.73 ± 8.23
Extracted power [N/Kg]	0.67 ± 0.133	0.86 ± 0.137
Thrust reduction [%]	6.22 ± 0.013	7.70 ± 0.013

Table 2: Extracted power and achievable thrust reduction

6.3 Phase plane

Since the phugoid mode is two-dimensional, we use a phase plane technique to analyze it ('Figure 14'). A switching surface (close to the null variation of airspeed axis) can be identified, seemingly regardless of the evolution of the turbulence disturbance. Even though further insights are needed, this result is linked to the similarity of the transfer functions from the wind to the energy derivative and the airspeed variation: they show identical phase plots but shifted by 180, thus the sign of the airspeed is always the opposite of the one of the energy derivative. Thanks to this nice property, the switch signal can be based on the airspeed evolution, thus reducing the number of sensors needed (there is no need to measure the total energy).

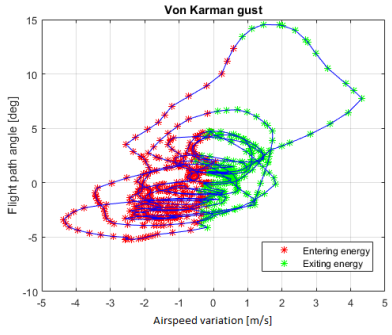

Figure 14: Phase plane of airspeed and flight path angle for Von Karman gust.

6.4 Energy gain dependence on the frequency of the gust

The control strategy that we developed is based on the difference on static gains between the entering and exiting energy transfer functions, that is at frequencies consistently lower than the phugoid one. In the frequency interval where the phase of the transfer functions is varying, we cannot foresee the performances of the control law. When the frequency of the gust gets consistently higher than the phugoid the "entering" and "exiting" transfer functions in 'Figure 8' are coincident, thus we expect that no energy extraction is achievable for that range. To check these observations, the whole controlled system is treated as input-output between the gust and the energy, and we scan on a set of gust frequencies the power extracted by the aircraft ('Figure 15'). A cutoff frequency is clearly identified and it is close to the phugoid frequency of the aircraft, meaning that we can extract energy from low frequency gusts and not from high frequency ones.

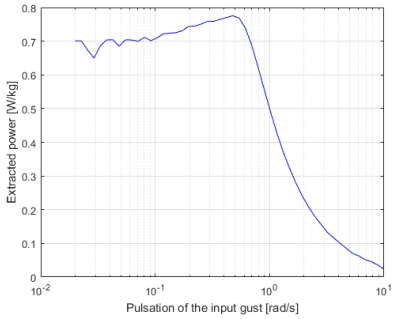

Figure 15: Power extraction capability depending on the frequency of the gust input.

7 CONCLUSIONS AND FUTURE WORK

First, we clearly presented the atmospheric gusty environment and described how much the gust spectrum can fit to the reality. Then we investigated the energy exchange mechanism between the wind and the aircraft. We proposed an innovative energy extraction control strategy based on a switching controller and we analyzed it. Energy savings between $5-10\%$ of the thrust needed during straight flight are achievable for realistic horizontal gusts and proven stability of the aircraft. Room for improvement is available, since it seems possible from numerical simulations to relax the stability limitations. This result is obtained without increasing considerably the control activity with respect to a stabilizing controller and with only the need of two sensors, one measuring the airspeed and one the flight path angle.

REFERENCES

[1] W.H.Phillips. Propulsive effects due to flight through turbulence. *Journal of Aircraft*, 12(7):867–871, 1975.

[2] T.Kiceniuk. Dynamic soaring and sailplane energetics. *Technical Soaring*, 25(4):221–227, 2001.

http://www.imavs.org/

http://www.imavs.org/

[3] T.Kiceniuk. Calculations on soaring in sink. *Technical Soaring*, 25(4):228–230, 2001.

[4] J.Bailey. Total energy control concepts applied to flight in windshear. In *AIAA Guidance, Navigation and Control conference, AIAA 1987-2344*, 1987.

[5] C.M.Belcastro and A.J.Ostroff. Total energy-rate feedback for automatic glide-slope tracking during wind-shear penetration. In *NASA technical paper 2412*, 1984.

[6] A.Lambregts. Vertical flight path and speed control autopilot design using total energy principles. In *AIAA Guidance and Control conference, AIAA 83-2239*, 1983.

[7] Z.Akos M.Nagy S.Leve and T.Vicsek. Thermal soaring flight of birds and unmanned aerial vehicles. *Bioinspiration and Biomimetics*, 5(4):045003, 2010.

[8] G.Sachs. Minimum shear wind strength required for dynamic soaring of albatrosses. *International Journal of Avaian Science*, 147(1):1–10, 2004.

[9] N.De Divitiis. Effect of microlift force on the performance of ultralight aircraft. *Journal of Aircraft*, 39(2):318–332, 2002.

[10] H.U.Mai. The effect of aeroelasticity upon energy retrieval of a sailplane penetrating a gust. *Technical soaring*, 10(4):62–72, 1985.

[11] N.Gavrilovic E.Benard P.Pastor and J.M.Moschetta. Performance improvement of small uavs through energy-harvesting within atmospheric gusts. In *AIAA Atmospheric Flight Mechanics Conference, AIAA 2017-1630, Grapevine, TX, USA*, 2017.

[12] J.W.Langelaan. Biologically inspired techniques for small and micro unmanned air vehicles. In *AIAA Guidance, Navigation and Control Conference and Co-located Conferences AIAA 2008-6511*, 2008.

[13] N.T.Depenbusch and J.W.Langelaan. Receding horizon control for atmospheric energy harvesting by small uavs. In *AIAA Guidance, Navigation and Control Conference, AIAA 2010-8177*, 2010.

[14] P.B.S.Lissaman and C.K.Patel. Neutral energy cycles for a vehicle in sinusoidal and turbulent vertical gusts. In *45th AIAA Aerospace Science Meeting and Exhibit, AIAA 2007-86*, 2007.

[15] H.Lee C.K.Patel and I.M.Kroo. Extracting energy from atmospheric turbulence. In *XXIX OSTIV Congress*, 2008.

[16] B.Etkin. *Dynamics of atmospheric flight, Chapter 13: Flight in a turbulent atmosphere*. John Wiley and sons, Toronto, 1972.

[17] I.Van Der Hoven. Power spectrum of horizontal wind speed in the frequency range from 0.0007 to 900 cycles per hour. *Journal of meteorology*, 14:160–164, 1956.

[18] T.Von Karman. Progress in the statistical theory of turbulence. *Proceedings of the National Academy of Sciences*, 34:530–540, 1948.

[19] J.C.Kaimal J.C.Wyngaard Y.Izumi and O.R.Coté. Spectral characteristics of surface-layer turbulence. *Quart. J.R. Met. Soc.*, 98(417):563–589, 1972.

[20] ESDU Data Item 85020. *Characteristics of atmospheric turbulence near the ground. Part II: single point data for strong winds (neutral atmosphere)*. Engineering Science Data Unit, London, UK, 2001.

[21] S.Watkins M.Thompson B.Loxton and M.Abdulrhaim. On low altitude flight through the atmospheric boundary layer. *International Journal of Micro Air Vehicles*, 2(2):55–68, 2010.

[22] P.P.Sukumar and M.S.Selig. Dynamic soaring of sailplanes over open fields. In *28th AIAA Applied Aerodynamics Conference, AIAA 2010-4953*, 2017.

[23] M.Abdulrahim and S.Watkins. Dynamic sensitivity to atmospheric turbulence of a fixed-wing mav with varying configuration. In *AIAA Guidance, Navigation and Control conference, AIAA 2009-5907*, 2009.

[24] F.Zhu and P.J.Antsaklis. Optimal control of switched hybrid systems: a brief survey. In *Technical report of the ISIS Group at the Univeristy of Notre Dame, ISIS-2013-007*, 2013.

[25] R.N.Shorten and K.S.Narendra. Necessary and sufficient conditions for the existence of a common quadratic lyapunov function for a finite number of stable second order linear time-invariant systems. *International Journal of adaptive control and signal processings*, 16(10):709–728, 2002.

APPENDIX A: COMPLETE LINEAR MODEL

The following matrices are the numerical values of the state space representation when considering the full linear model.

$$A^{complete} = \begin{bmatrix} -0.049 & -9.81 & -1.79 & -0.061 & 0 & 0 & 0 \\ 0.049 & 0 & 6.78 & 0.023 & 0 & 0 & 0 \\ -0.049 & 0 & -6.78 & 0.98 & 0 & 0 & 0 \\ 0 & 0 & -31 & -2.57 & 0 & 0 & 0 \\ 0 & -20 & 0 & 0 & 0 & 0 & 1 \\ 0 & 0 & 0 & 0 & 0 & 0 & 0 \\ 0 & 0 & 0 & 0 & 0 & 0 & 0 \end{bmatrix}$$

$$B^{complete} = \begin{bmatrix} 1 & -0.119 & -1 & 0 \\ 0 & 0.453 & 0 & 0.05 \\ 0 & -0.453 & 0 & -0.05 \\ 0 & -49.2 & 0 & 0 \\ 0 & 0 & 0 & 0 \\ 0 & 0 & 1 & 0 \\ 0 & 0 & 0 & 1 \end{bmatrix}$$

$$C^{complete} = \begin{bmatrix} 20 & 0 & 0 & 0 & -9.81 & 20 & 0 \end{bmatrix}$$

APPENDIX B: PHUGOID APPROXIMATION OF THE DAMPED AIRCRAFT

The phugoid approximation of the damped system is obtained by reducing the (fast) short period mode states, which is a standard technique. We obtain the following state space matrices.

$$A_{damped}{}^{phugoid} = \begin{bmatrix} -0.044 & -9.6 & 0 & 0 & 0 \\ 0.029 & -0.73 & 0 & 0 & 0 \\ 0 & -20 & 0 & 0 & 0 \\ 0 & 0 & 0 & 0 & 0 \\ 0 & 0 & 0 & 0 & 0 \end{bmatrix}$$

$$B^{phugoid} = \begin{bmatrix} 1 & 1.18 & -1 & 0 \\ 0 & -6.7 & 0 & 0.05 \\ 0 & 0 & 0 & 0 \\ 0 & 0 & 1 & 0 \\ 0 & 0 & 0 & 1 \end{bmatrix}$$

$$C^{phugoid} = \begin{bmatrix} 20 & 0 & -9.81 & 20 & 0 \end{bmatrix}$$